European Journal of Mechanics / A Solids 96 (2022) 104739

Contents lists available at ScienceDirect

European Journal of Mechanics / A Solids

journal homepage: www.elsevier.com/locate/ejmsol

Corrosion-fatigue crack growth behaviour of wire arc additively manufactured ER70S-6 steel parts in marine environments

Anna Ermakova [a], Supriyo Ganguly [b], Javad Razavi [c], Filippo Berto [c], Ali Mehmanparast [a,*]

[a] Department of Naval Architecture, Ocean and Marine Engineering, University of Strathclyde, Glasgow, G1 1XQ, United Kingdom
[b] Welding Engineering and Laser Processing Centre, Cranfield University, Cranfield, MK43 0AL, UK
[c] Department of Mechanical and Industrial Engineering, Norwegian University of Science and Technology (NTNU), Trondheim, Norway

A B S T R A C T

A crucial part of the structural integrity assessment of marine structures is the analysis of the fatigue crack growth behaviour of the welded joints in seawater environments, where the cracks often initiate and propagate under corrosion-fatigue loading conditions. In recent years, technological developments have facilitated the fabrication of steel components and structures using additive manufacturing technologies. Among the existing technologies, the Wire Arc Additive Manufacturing (WAAM) technique has proven to offer great potentials for fabrication of large-scale structures. The present study investigates the corrosion-fatigue crack growth (CFCG) behaviour of the WAAM parts fabricated using ER70S-6 low carbon steel wire to assess the suitability of this technology for future marine structures. In this experimental study, the cracking behaviour and test duration in corrosion-fatigue tests were investigated and analysed in conjunction with the microstructural examination of the tested specimens. Moreover, the obtained results were compared with the recommended trends available in BS7910 standard for conventional welded joints and the data available in the literature on widely used offshore structural steel weldments. The CFCG results obtained from this study contribute to the overall knowledge and design requirements for the new optimised functionally graded structures made with WAAM technology for marine applications.

1. Introduction

Offshore wind turbine foundations, which are fabricated using conventional welding techniques, experience millions of load cycles during their service life in highly corrosive environments. Therefore, under corrosion-fatigue loading conditions the welded joints in these marine structures are often found to be the potential areas for crack initiation and propagation which can eventually lead to catastrophic failure of the structure (Mehmanparast et al., 2018). Moreover, the phase changes in metal, induced during the welding process can change the pattern of crack growth mechanisms, introducing crack branching (Adedipe et al., 2017). Some studies on the heat affected zones (HAZ) of welded wrought steels confirm that the fatigue crack growth (FCG) rates strongly depend on the welding procedure, alloy composition, crack growth region, residual stress magnitude and distribution, and service environment (Burnside et al., 1984; Adedipe et al., 2016; Fatigue behaviour of high, 2679; Bertini, 1991). These studies suggest that the material selection and fabrication technology have a significant impact on the design life of the marine structures and the fatigue life of these structures can be considerably enhanced by employing more damage tolerant materials and appropriate manufacturing techniques.

Wire arc additive manufacturing (WAAM) technique is a relatively new additive manufacturing (AM) technology that enables the production process by feeding a wire of metal into an electric arc to melt the material on top of the previously deposited layers at a controlled rate. The key advantages of this method compared with widely used powder-based AM methods, are large-scale near net shape parts that can be fabricated at acceptable cost, in reasonable time with deposition rates of several kilograms per hour (Zhang et al., 2017; Martina et al., 2012; Williams et al., 2015). However, as the WAAM process consists of complex welding thermal cycles, it will lead to microstructural variations and introduce a complex and variably distributed residual stress state. This will have profound influence on the overall mechanical behaviour of a WAAM built part (Liljedahl et al., 2009; Xu et al., 2018). While the employment of the WAAM technique in some industries, such as aerospace, has been widely investigated in recent years, the great potentials that this AM technique offers make it a suitable manufacturing technology for many other industrial sectors such as renewable energy marine structures. In order to investigate the suitability of the WAAM technique for employment in fabrication and repair of renewable energy marine structures, the corrosion-fatigue crack growth (CFCG) behaviour of a WAAM built steel part needs to be accurately characterised and compared to the conventional welded joints. This will provide an insight into the estimation of the remaining lifetime and development of efficient inspection plans for future WAAM

* Corresponding author.
E-mail address: ali.mehmanparast@strath.ac.uk (A. Mehmanparast).

https://doi.org/10.1016/j.euromechsol.2022.104739
Received 7 October 2021; Received in revised form 7 July 2022; Accepted 11 July 2022
Available online 14 July 2022
0997-7538/© 2022 The Author(s). Published by Elsevier Masson SAS. This is an open access article under the CC BY license (http://creativecommons.org/licenses/by/4.0/).

Nomenclature

a_0	Initial crack length in C(T) specimen
a_i	Instantaneous crack length
$a_{i,p}$	Crack length after pre-fatigue cracking
$a_{f,c}$	Final crack length (compliance data)
$a_{f,op}$	Final crack length (fracture surface)
B	Total thickness of C(T) specimen
C	Material constant for fatigue crack growth
da/dN	Fatigue crack growth rate
H	C(T) specimen height
K_{max}	Stress intensity factor corresponding to P_{max}
ΔK	Stress intensity factor range
m	Material constant for fatigue crack growth
P_{max}	Maximum load in fatigue cycles
P_{min}	Minimum load in fatigue cycles
R	Load ratio
R ()	Coefficient of determination
W	C(T) specimen width
AM	Additive Manufacturing
B	Bottom
BFS	Back Face Strain measurement technique
BM	Beach Marking
CFCG	Corrosion-fatigue crack growth
C(T)	Compact Tension specimen
CMT	Cold Metal Transfer
EDM	Electrical Discharge Machining
FCG	Fatigue Crack Growth
H	Horizontal
HAZ	Heat Affected Zone
SIF	Stress Intensity Factor
SD	Standard Deviation
T	Top
V	Vertical
WAAM	Wire Arc Additive Manufacturing

built marine structures and components.

The environmental behaviour of low carbon steel ER70S-6 specimens produced by means of WAAM was examined by Ron et al. (2019), where general corrosion performance was evaluated by salt spray testing, immersion testing, potentiodynamic polarization analysis, and electrochemical impedance spectroscopy. The stress corrosion performance was also assessed by slow strain testing. The results have shown that the general and stress corrosion resistance of WAAM specimens was similar with the ST-37 steel counterparts. Therefore, it was concluded that the WAAM process does not cause any further deterioration in corrosion performance when compared with the conventional wrought alloy. A similar research study was conducted on austenitic stainless steel WAAM built parts (Ron et al., 2021), which also showed that electrochemical performance and stress corrosion susceptibility of the parts were similar with the wrought counterparts, despite differences in microstructure and mechanical properties. Moreover, the effect of microstructure imperfections on corrosion-fatigue performance of the material was evaluated for ER70S-6 WAAM parts in a 3.5% NaCl solution (Ron et al., 2020). The results presented a reduction in fatigue strength of WAAM specimens, compared to the wrought ST-37 counterparts, due to porosity, impurities and lack of fusion defects that are imposed during WAAM production process and promote corrosion attacks and consequently stimulate fatigue cracking.

It is evident from previous studies that the WAAM process introduces microstructural variation in additively built parts compared with wrought steel. These changes directly affect the behaviour of WAAM built steel parts, including their corrosion characteristics, hence require additional in-depth studies. Although some limited studies were previously performed on the structural response of the WAAM built parts in corrosive environments, no trends nor comprehensive studies on the CFCG of the WAAM built parts are currently available in the literature. Therefore, the present study focuses on the investigation of the CFCG behaviour of ER70S-6 low carbon steel WAAM built specimens in seawater. Moreover, an experimental sensitivity analysis has been conducted on the corrosion-fatigue response of the material to the build location and cracking orientation. The WAAM strategy adopted in this study, the CFCG test set-up, the crack growth monitoring method employed in this study, data collection process and analysis, and comparison with the existing data in the literature are presented and discussed in the following sections. The results presented in this study demonstrate the possibility of employment of the WAAM process for offshore structures with harsh environmental conditions such as offshore wind, where the structures experience severely high number of cycles in corrosive environments.

2. Manufacturing set-up and specimen extraction

For this study a WAAM wall was manufactured with Lincoln electric ER70S-6 welding filler wire with the chemical composition specified in Table 1, using the Cold Metal Transfer (CMT) process. The fabrication parameters for the WAAM wall are shown in Table 2. The full manufacturing set-up and the completed WAAM wall are shown in Fig. 1. It can be seen in this figure that the set-up comprises of a CMT power source, a robotic arm with the torch that is feeding the wire and supplying the shielding gas at the same time. An exhaust fan was used to remove any fume and cool the wall from the excessive heat generated during the manufacturing process.

The WAAM wall was built on top of a base plate, which was made of EN10025 rolled structural steel, with dimensions of 420 × 200 × 12 mm^3. The deposition was carried out in the middle of the base plate using an oscillation deposition pattern (Ermakova et al., 2019, 2020). The wall was built with the following dimensions: thickness of 24 mm (Y-axis in Fig. 1 (b)), length of 355 mm (X-axis) and height of 140 mm (Z-axis). The base plate was rigidly fixed on the work table with eight clamps, to prevent bending and distortions of the base plate due to the increased temperature. The clamps were released once the WAAM wall deposition was completed and it was cooled down to the ambient temperature.

Upon completion of the WAAM wall, four notched compact tension, C(T), specimens were extracted using Electrical Discharge Machining (EDM) technique. The specimens were extracted from two locations: top (T) and bottom (B), and in two orientations: vertical (V) – with crack plane perpendicular to the additive layers, and horizontal (H) – with crack plane parallel to deposited layers. These four combinations provided specimens denoted CT-VT, CT-VB, CT-HT and CT-HB as schematically shown in Fig. 2 (a). The C(T) specimens were designed according to ASTM E647 standard (ASTM E647 – 13, 2014) with a width of $W = 50$ mm, height of $H = 60$ mm, total thickness of $B = 16$ mm and initial crack length of $a_0 = 17$ mm. Knife edges were machined at the crack mouth of the C(T) specimens following the guidelines in ASTM E1820 standard (American Society for Testing and Materials, 2011) to accommodate a clip gauge for compliance measurements during fatigue pre-cracking, which is required to introduce an infinitely sharp crack tip ahead of the machined notch prior to CFCG testing. All four specimens were pre-cracked under fatigue loading conditions using the load decreasing approach to approximately 20 mm ($a_{i,p}/W = 0.4$). It is worth noting that the final value of maximum stress intensity factor K_{max} at the end of pre-cracking did not exceed the initial K_{max} at the beginning of the actual CFCG test. During the main CFCG tests, the crack growth

Table 1
Chemical composition of ER70S-6 material (wt.-%) (Lincoln Electric Company and T).

	C	Mn	Cr	Si	Ni	Mo	S	P	Cu	V
ER70S-6	0.09	<1.60	0.05	0.09	0.05	0.05	0.007	0.007	0.20	0.05

Table 2
CMT-WAAM fabrication parameters.

Shielding gas	Ar+20% CO_2
Gas flow rate	15 L/min
Wire diameter	1.2 mm
Wire feed speed	7.5 m/min
Robot travelling speed	7.33 mm/s
Dwell time	120 s

monitoring was performed using the back face strain measurement technique (see Fig. 2 (b)) the details of which are described in section 3.

3. Corrosion-fatigue crack growth test set-up and data analysis

3.1. Test set-up

CFCG tests were performed on C(T) specimens under load-controlled mode using a 100 kN servo hydraulic Instron machine. The sinusoidal cyclic load was applied under a constant amplitude with the maximum load of $P_{max} = 10$ kN, the load ratio of $R = 0.1$, and frequency of $f = 0.3$ Hz, which is the typical frequency used in corrosion-fatigue analysis for offshore structures (Henderson, 2003; Jacob et al., 2019). To simulate free-corrosion conditions for the tests, 60 L of artificial seawater was prepared according to ASTM D1141-98 (International, 2013), using deionised water and chemicals shown in Table 3. The pH level of seawater was maintained at 8.0–8.2 during the tests, and once it dropped below 8.0 the seawater was subsequently replaced. The full CFCG test set-up is shown in Fig. 3 (a). The test specimen was placed in an environmental water chamber that was attached onto the machine, with the area of interest within the crack path immersed in seawater throughout the test (Fig. 3 (b)). The created artificial seawater stored in a tank was running through the water chamber using pumps at a continuous rate of 4 L/min to create a circulation of simulated seawater during the test. The seawater temperature was controlled using a chiller and varied between 8.0 and 10.0 °C to replicate the operation conditions in the North Sea.

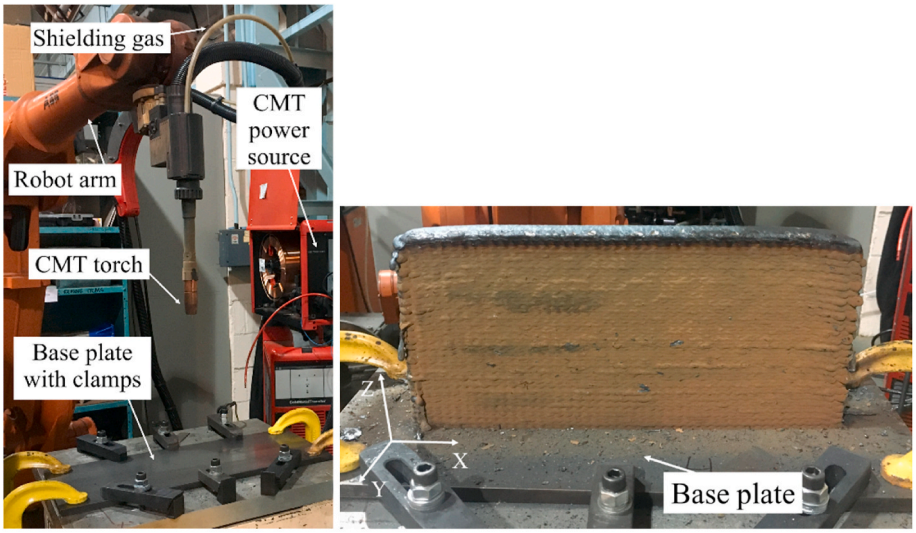


Fig. 1. Fabrication process (a) CMT WAAM set-up, (b) completed WAAM wall.

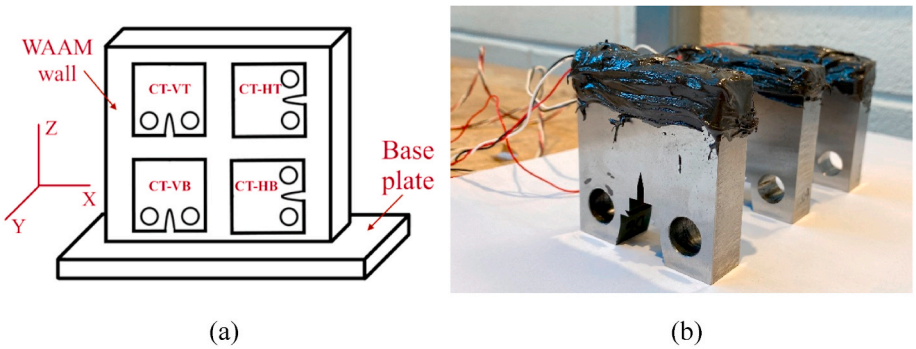


Fig. 2. Specimens (a) extraction plan from the WAAM wall, (b) in protective coating after strain gauging.

Table 3
Chemical composition of artificial seawater (International, 2013).

Chemical compound	Concentration (g/L)
$NaCl$	24.53
$MgCl_2$	5.20
Na_2SO_4	4.09
$CaCl_2$	1.16
KCl	0.695
$NaHCO_3$	0.201
KBr	1.101
H_3BO_3	0.027
$SrCl_2$	0.025
NaF	0.003

3.2. Crack growth monitoring methods

An efficient crack growth monitoring technique that is suitable for corrosion-fatigue tests, where the specimen is soaked in seawater with limited direct access to it, is the back face strain (BFS) method (Adedipe et al., 2015; Newman et al., 2011). The main idea in this approach, which is originally designed for CFCG testing on C(T) specimens, is to correlate the BFS variations with the crack length. These empirical correlations, which are generally referred to as BFS calibration curves, are initially developed in air for a given loading condition and then used in CFCG tests in seawater to estimate the instantaneous crack length throughout the test using the collected BFS data. The BFS values are recorded from the strain gauge attached to the back of the C(T) specimens at the mid-height and mid-width. The basis of this approach is similar to the compliance measurement technique in FCG tests in air where the instantaneous crack length is estimated using the crack mouth displacement data. Therefore, for a given material, specimen geometry and testing condition, the BFS and crack mouth displacement (hence compliance) data are directly correlated, and the instantaneous crack length can be estimated using the data which can be collected from the test depending on the access limitations to the test specimen (i.e. immersed specimen in seawater).

After attaching strain gauges onto the C(T) specimens in the present study, a polysulfide coating was applied to protect the specimens against seawater damage (Fig. 2 (b)) and then the specimens were soaked in seawater for approximately 24 h prior to testing, as recommended by ASTM D1141 (International, 2013). The BFS values from the strain gauge attached to the back of the specimen were recorded with a strain recorder every second and the maximum magnitude of compressive strain values were captured with a camera every minute (Fig. 3 (a)). Prior to CFCG testing, four calibration tests were performed in air on C (T) specimens with the same dimensions and extraction orientations/locations (VT, HT, VB, HB), under loading conditions presented in Table 4, to generate empirical BFS calibration curves for each of the four ER70S-6 WAAM specimens. It can be noted here, that due to dependency of BFS calibration curves on the load level, the applied loads for the calibration tests in air and CFCG tests in seawater were the same. The tests in air were conducted using a clip gauge attached to the knife edges at the crack mouth of the C(T) specimens for instantaneous crack length measurements, which were then correlated with the maximum magnitude of compressive BFS value (hence maximum crack mouth opening). Four calibration curves were derived by applying cubic polynomial lines of best fit to the data and then used to correlate the BFS recordings from seawater tests with the estimated instantaneous crack lengths for each case.

Moreover, beach marking (BM) was carried out at different intervals throughout the tests to cross-check the accuracy of the estimated crack length from the BFS technique (Hou, 2007). In this method, the maximum cyclic fatigue load and frequency are decreased for a limited period of time to introduce thin marks on the fracture surface, so called beach marks. By recording the BFS value at which the beach marking process was applied, the estimated crack lengths can be verified through comparison with the experimentally measured crack length on the fracture surface subsequent to completion of the test. In order to apply the BM in these tests, the loading conditions were changed to $P_{max} = 8$ kN with the load ratio of $R = 0.125$ and frequency of $f = 0.1$ Hz for 1 h to perform beach marking in the absence of noticeable crack growth (this was confirmed by ensuring that the BFS values remained constant during beach marking procedure). For each CFCG test, this process was performed three times to introduce multiple BM data for further validation of the calibration curves. The BM approach was initially employed in BFS calibration tests in air on nominally identical C(T) specimens to verify the accuracy of crack length estimations, the results and loading conditions of which are presented in Fig. 4 and Table 4, respectively. For the CFGC tests in seawater, to make beach marks more visible and keep them at sufficient distance from each other, every

Table 4
Beach marking loading conditions for the tests in air and seawater.

Test environment	The main test condition			Beach marking loading condition		
	P_{max} (kN)	R	f (Hz)	P_{max} (kN)	R	f (Hz)
Air	10	0.1	5	8	0.125	3
Seawater	10	0.1	0.3	8	0.125	0.1

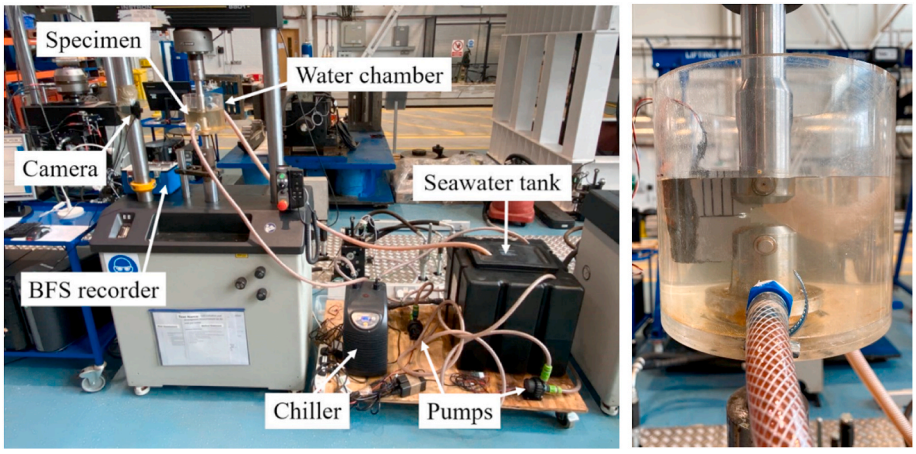


Fig. 3. CFCG test (a) full set-up, (b) specimen in the water chamber.

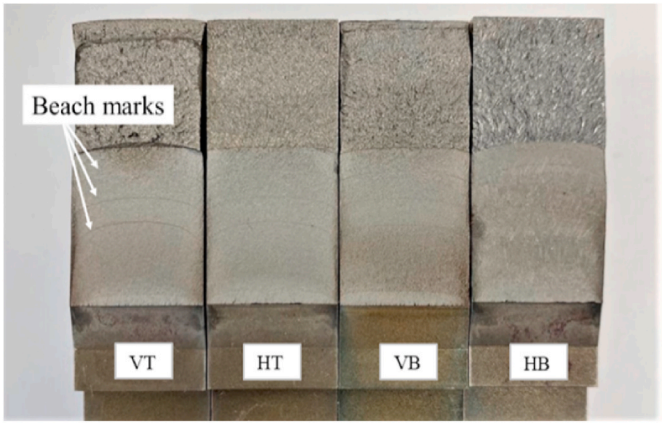


Fig. 4. The beach marks on fracture surface of WAAM ER70S-6 C(T) specimens tested in air.

specimen was marked prior to testing, dividing the required 15 mm of the crack length into three regions (5 mm each) as shown in Fig. 3(b). Crack length was visually inspected throughout the test and when it was approximately in the middle of each marked region, BM was employed. The CFCG tests were terminated once the crack length reached 15 mm ($a_{f,c}/W = 0.7$).

After completion of the CFCG tests, all four C(T) specimens were broken open to measure the actual crack lengths on the fracture surface and verify the accuracy of the estimated crack lengths from the BFS data. In order to break open the specimens post-testing, the specimens were initially soaked in liquid nitrogen for 5 min to induce brittleness in the specimens (thereby minimising any deformation during the breaking process) and then pulled in tension using a servo hydraulic Instron machine. The fracture surfaces of all four CFCG specimens are displayed in Fig. 5. It is worth noting here that due to the corroded fracture surface the beach marks were not very clear (see Fig. 5) compared with the specimens tested in air (see Fig. 4), so some level of error in measurements might be expected when the beach marks are measured in corrosion-fatigue test specimens. In Fig. 5, three distinct areas corresponding to different stages of the test can be clearly identified on the fracture surfaces: (1) fatigue pre-cracking, (2) fatigue crack growth, and (3) fast fracture (i.e. specimen fracture opening). Also from Fig. 5 it can be concluded that the crack propagation regions are symmetric in all four C(T) specimens, indicating good alignment during the CFCG tests. An example of the calibration curve for CT-HB specimen tested in seawater, plotted using the empirical correlation from the air test, is shown in Fig. 6. It can be seen in Fig. 6 that the calibration curve and beach marking results are in good agreement, hence the estimated crack lengths using the BFS data are fairly reliable.

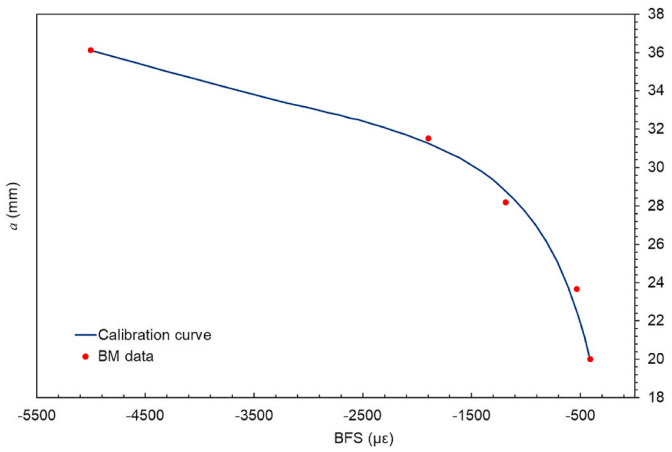


Fig. 6. Crack length vs. BFS values for CT-HB specimen tested in seawater, and the comparison with the beach marking data.

3.3. Data analysis

The CFCG rate, da/dN, was calculated using the estimated crack lengths and the number of cycles, using the secant method for the first and the last three data points, and seven-point incremental polynomial technique for the rest of the data points. The stress intensity factor (SIF) was determined using the shape function equation developed by Mehmanparast et al. (2017), Equation (1), that offers accurate solutions for a wider range of crack length in a C(T) specimen, $0.2 = a/W \leq 0.7$, compared with the original shape function equation available in ASTM E647 standard. In the SIF calculation shown in Equation (1), α is the normalised crack length a/W and ΔP is the load range which is defined as the difference between the maximum load P_{max} and the minimum load P_{min}.

$$\Delta K = \frac{\Delta P}{BW} \bullet \sqrt{a} \bullet \left(-372.12\alpha^6 + 1628.60\alpha^5 - 2107.46\alpha^4 + 1304.65\alpha^3 - 391.20\alpha^2 + 54.81\alpha + 7.57 \right) \quad (1)$$

4. Test results and discussion

The estimated crack lengths for each tested specimen were plotted against the number of cycles and the results are shown in Fig. 7. It can be observed in this figure that the longest fatigue life (i.e. largest number of cycles) was experienced in the vertical specimen that was extracted from top of the WAAM wall CT-VT. Fig. 7 shows that this specimen endured approximately 1.5–1.7 times more cycles to reach 15 mm of crack extension compared to other specimen locations/orientations. Another observation that can be made from this figure is that the test durations

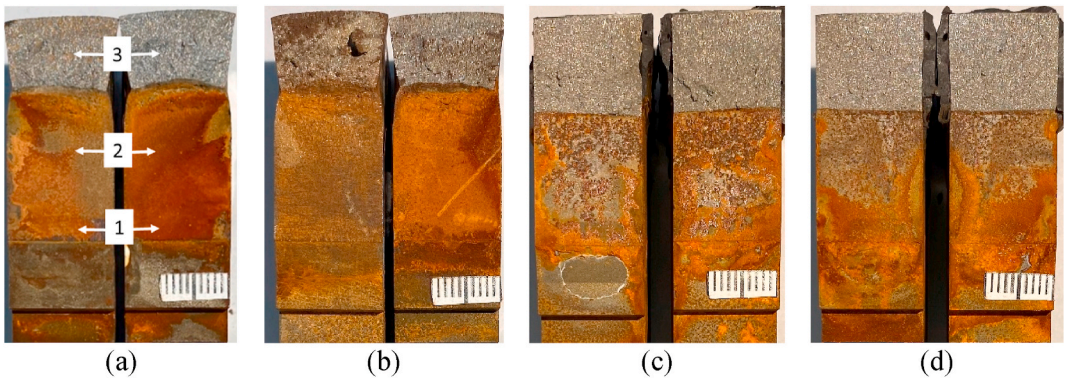


Fig. 5. Fracture surface of WAAM built ER70S-6 specimens after CFCG test (a) CT-VT, (b) CT-VB, (c) CT-HT, (d) CT-HB (each division on the scale bars indicates a distance of 1 mm).

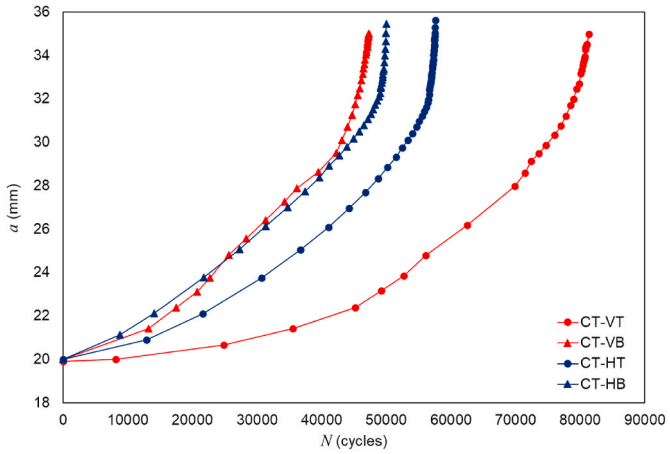


Fig. 7. Corrosion-fatigue crack growth trends in ER70S-6 WAAM built specimens.

for the two specimens extracted from the top of the wall, regardless of their orientation, is the longest compared to the specimens from the bottom of the wall. The longer fatigue life in the specimens extracted from the top of the WAAM wall would have been caused by the microstructural variations caused by different thermal effects and presumably the residual stresses induced during WAAM fabrication process which are expected to have higher magnitudes of compressive residual stress in the top layers compared to the bottom layers due to the greater number of repeated thermal cycles. The two specimens extracted from the bottom part of the WAAM wall show similar results with the average number of cycles of around 49,000 to reach 15 mm of crack extension. Comparison of CFCG behaviour of ER70S-6 WAAM walls with the FCG test results in air conducted in a previous study by Ermakova et al. (2021) shows that whilst the fatigue life is more dependent on the orientation of the specimens in air tests, for seawater tests the extraction location has a more pronounced effect on the fatigue life of the test specimens. These observations indicate that the fatigue test duration of ER70S-6 WAAM built specimens strongly depends on the test environment.

The CFCG rates, *da/dN*, for all C(T) specimens have been then correlated with the linear elastic fracture mechanic parameter, *ΔK*, and the results are displayed in Fig. 8. This figure illustrates the typical environmental crack growth behaviour, where the crack growth rate, *da/dN*, is highly sensitive to the applied *K* in Stage I and Stage III. It can be observed in this figure that while in Stage II the crack growth rate increases with an increase in *ΔK*, the slope of the *da/dN* versus *ΔK* curve

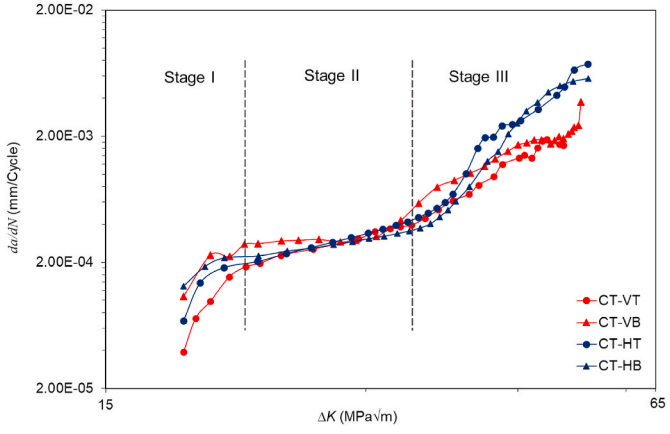


Fig. 8. Corrosion-fatigue crack growth rates for ER70S-6 WAAM built specimens.

in this stage is much lower than in Stage I and III. Moreover, it can be seen that the slope of CT-VB specimen in Stage II is almost insensitive to the applied *ΔK* and the *da/dN* for this specimen is almost constant in Stage II. Further observed in Fig. 8 is that in Stage I and II, the CFCG data for the same specimen extraction locations (Top or Bottom) fall close to each other within the inherent experimental scatter; however, towards the end of the test (i.e. in Stage III) the vertical specimens have noticeably lower crack growth rates than the horizontal specimens, regardless of their extraction locations. It is worth noting here that the lowest CFCG rates in Stage I and III are obtained from the vertical specimen extracted from the top of the wall, CT-VT; however, in Stage II, all four datasets fall close to each other with the specimens with the same extraction locations falling almost upon each other. Comparison of the CFCG results in seawater from the present study with the results from the air tests reported by Ermakova et al. (2021) shows that under similar loading conditions the specimen orientation has a higher impact on the crack growth behaviour of the material in the air tests, with vertical specimens presenting higher trends throughout the test than the horizontal specimens. Whereas in seawater environment the crack growth behaviour changes depending on the stage of the test. Since only four CFCG specimens were tested in this study, with four different combinations of extraction locations and orientations, further tests must be conducted in future work to confirm the provisional trends presented in this study and evaluate the level of scatter for each specimen. Moreover, the residual stresses need to be measured to evaluate their effects on the crack growth behaviour for each specimen location/orientation.

Further analysis was carried out on Stage II (Paris region) data points obtained from all four tests, and the material constants *C* and *m* (see Equation (2)) were determined for each dataset by plotting the line of best fit and extracting the power-law constants. The Paris law constants obtained from each data set are summarised in Table 5. In addition to *C* and *m* constants, the values of the coefficient of determination, R^2, were also calculated to examine how accurately the lines of best fit describe the material behaviour. As seen in Table 5 the R^2 values for all tests are close to 1 except CT-VB specimen where the crack growth rate is almost constant during Stage II (see Fig. 8).

$$da / dN = C\Delta K^m \tag{2}$$

Additionally, the Paris law constants were obtained for specimens with the same extraction location (top or bottom) and the results are shown in Fig. 9 and Table 6. With closer look in Fig. 9, a difference in slopes for Set-T (all specimens extracted from the top of the wall) and Set-B (all specimens extracted from the bottom of the wall) can be observed, where Set-B is less sensitive to the applied *ΔK*. Also, Set-B has higher level of scatter between two sets of data, which is confirmed by R^2 values from the table. The level of scatter was further analysed by calculating the upper bound trends for two location datasets, based on mean +2 standard deviation (SD), the material constants for which were

Table 5
Paris law constants obtained from the CFCG tests performed on ER70S-6 WAAM built specimens (*da/dN* in mm/Cycle and *ΔK* in MPa$\sqrt{m}$).

Specimen ID	Orientation	Location	P_{max} (kN)	*C*	*m*	*R* (Adedipe et al., 2017)
CT-VT	Vertical	Top	10	7.85×10^{-7}	1.77	0.994
CT-VB	Vertical	Bottom	10	1.13×10^{-4}	0.296	0.679
CT-HT	Horizontal	Top	10	5.89×10^{-7}	1.87	0.993
CT-HB	Horizontal	Bottom	10	5.15×10^{-6}	1.21	0.983

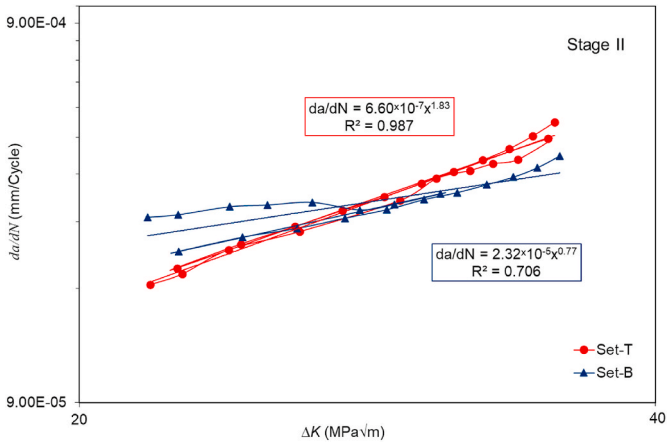


Fig. 9. Lines of best fit made to the CFCG data in Stage II region for different specimen locations (Set-T for top specimens and Set-B for bottom specimens).

Table 6
Power law constants for the mean curves and upper bound trends in Stage II region for different specimen location datasets.

Datasets	Location	P_{max} (kN)	Mean			Mean + 2SD	
			C	m	R (Adedipe et al., 2017)	C	m
Set-T	Top	10	6.60 × 10^{-7}	1.83	0.987	7.06 × 10^{-7}	1.83
Set-B	Bottom	10	2.32 × 10^{-5}	0.77	0.706	2.71 × 10^{-5}	0.77

added into Table 6.

The mean + 2SD lines for two datasets of top and bottom specimens are plotted in Fig. 10, along with the BS7910 recommended upper bound trends for welded joints tested in seawater (BS 7910, 2015), based on the simplified law and the 2-stage law. It can be seen from this figure that both upper bound lines describing the behaviour of tested specimens fall below the BS7910 recommended lines, indicating that the CFCG rates of WAAM ER70S-6 components can be conservatively predicted by the recommended trends in the standard.

Moreover, the CFCG rates obtained in this study have been compared with the experimental data available on welded steel specimens tested in seawater, such as: S355G10+M structural steel C(T) specimens extracted from the heat affected zone (HAZ) (Jacob and Mehmanparast, 2021), S355G8+M steel C(T) specimens extracted from HAZ and base metal (Mehmanparast et al., 2017), S355J2+N steel C(T) specimens extracted from HAZ (Adedipe et al., 2017) and weld areas and X70 pipeline steel specimens (Vosikovsky, 1980). All tests were carried out under similar loading conditions as summarised in Table 4 and are presented in Fig. 10. Comparison of all experimental curves shows that the upper bound lines obtained from this study for WAAM ER70S-6 specimens fall slightly above the experimental trends for S355G10+M, S355G8+M and S355J2+N HAZ specimens; however, they are below the curve for X70. The slope for ER70S-6 Set-T specimens replicates the slopes for curves representing the behaviour of S355G10+M HAZ specimens. Since S355G10+M, S355G8+M and S355J2+N steels are widely used in fabrication of offshore structures, which are subjected to severe cyclic loads in harsh marine environments, the comparison from Fig. 10 confirms that the WAAM technology and ER70S-6 steels can be potentially considered for fabrication of offshore structures, even though its corrosion-fatigue cracking resistance is slightly less than S355 welded steels, but the crack growth rates are still below the recommended CFCG trends provided in BS7910 standard. In addition to the fracture mechanics studies performed in this study, S–N fatigue tests will also need to be conducted in future work to assess the design requirements of WAAM built components for operation under cyclic loading marine conditions. Further comparison of the test duration from this study to four tests on S355G10+M HAZ specimens performed by Jacob et al. (Jacob and Mehmanparast, 2021) shows that on average it takes three times longer to propagate the crack to 15 mm in WAAM ER70S-6 specimens than in the wrought counterparts.

5. Microstructural examinations

Due to the severe level of corrosion developed on the fracture surface of the specimens during the CFCG tests (see Fig. 5), microscopical examination of fracture mechanisms was not possible for the specimens tested in this study. However, a thin slice of approximately 1.5 mm thickness was removed from the fracture surface using EDM technique to examine the microstructure of each specimen underneath the fracture surface. Each specimen slice was prepared for microstructural analysis according to ASTM E407-07 standard (Practice and S, 2016) by hot-mounting in a mould, followed by grinding, polishing and finally etching using 2% Nital solution for 10 s. Then the microstructures of the specimens in the areas corresponding to the middle of Paris regions were examined using a HIROX RH-2000 digital microscope, and the results

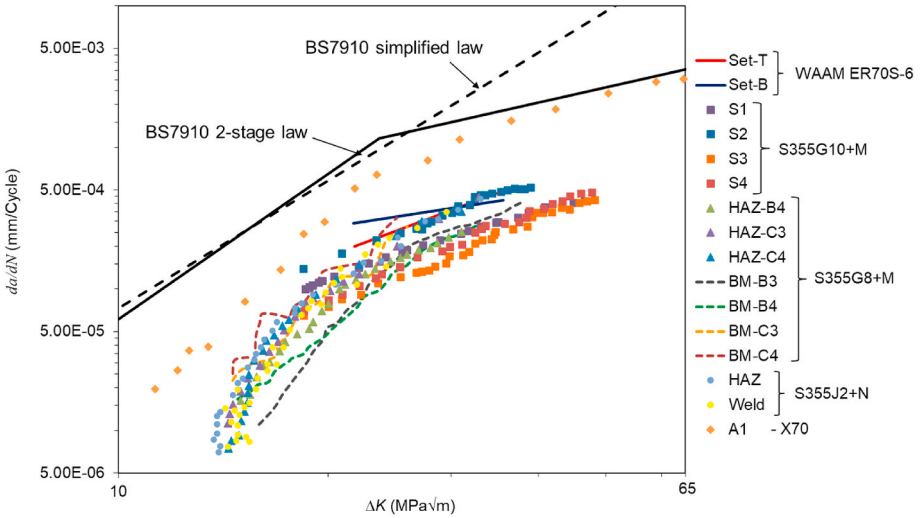


Fig. 10. Comparison of the upper bound CFCG trends for ER70S-6 WAAM specimens with BS7910 curves and the literature data on structural steels.

are presented in Fig. 11. These figures reveal a typical microstructure for low carbon steel that consists of a ferrite matrix and reduced amount of a secondary pearlite phase due to low amount of carbon in metal composition (Table 1) and rapid solidification process of WAAM. Similar results were presented in several research studies by Ron et al., 2019, 2020. Comparison of the micrographs for four specimens in Fig. 11 shows that no distinct difference can be observed in the grain structure of the specimens tested in this study.

The general microstructure, at lower magnification, for vertical and horizontal specimens captured from the extracted slice underneath the fracture surface is shown in Fig. 12. As seen in this figure, the microstructure of the horizontal specimens with the crack path located within a single deposited layer is relatively uniform as expected (Fig. 12 (b)) compared to the non-uniform grain structure of the vertical specimens with multiple deposited layers (Fig. 12 (a)), where clear boundaries can be observed between AM layers. It can be clearly seen in Fig. 12 (a) that a grain size variation is present along the crack path which can subsequently influence the cracking behaviour of the vertical specimens. It was previously reported that the grain refinement, shown in vertical specimens, can result in toughness improvement and hence the material can be expected to have higher cracking resistance through the weld region, affecting the crack growth rates in that region (Adedipe et al., 2017).

6. Conclusions

Corrosion-fatigue crack growth tests were carried out in artificial seawater on standard C(T) specimens extracted from WAAM built walls made with ER70S-6 wire low carbon steel. All tests were conducted at load level of $P_{max} = 10$ kN, with $R = 0.1$, and frequency of 0.3 Hz. The following observations and conclusions can be made from this study:

- The specimen extraction location with respect to the WAAM wall affects the duration of the test and the CFCG rates particularly in Stages I and II. The specimens extracted from the top of the WAAM wall required on average 1.4 times more cycles to reach 15 mm of crack extension compared to those from the bottom of the wall.
- The orientation of the extracted specimens may have minor effects on the CFCG rates towards the end of the test in Stage III.
- The lowest CFCG rates in Stage I and III were exhibited in the vertical C(T) extracted from the top of the wall while in Stage II all four results fall close to each other.
- The mean + 2SD lines for top and bottom specimen datasets fall below the BS7910 recommended fatigue crack growth trends, slightly higher than S355G8+M and S355G10+M HAZ data sets but below X70.
- The ER70S-6 WAAM built specimens require on average three times greater number of cycles to propagate the crack to 15 mm compared to the wrought counterparts extracted from S355G10+M HAZ steel.
- Further tests need to be examined in future work to evaluate the level of scatter in the data. Moreover, the influence of the residual stresses in C(T) specimens on the CFCG behaviour of the WAAM built specimens need to be considered and analysed in future work.

Author statement

Anna Ermakova: Methodology, Validation, Formal analysis, Writing – original draft; **Supriyo Ganguly**: Resources, Writing – review & editing; **Javad Razavi**: Conceptualization, Validation, Writing – review & editing; **Filippo Berto**: Conceptualization, Writing – review & editing; **Ali Mehmanparast**: Conceptualization, Resources, Writing – review & editing, Supervision.

Declaration of competing interest

The authors declare that they have no known competing financial interests or personal relationships that could have appeared to influence the work reported in this paper.

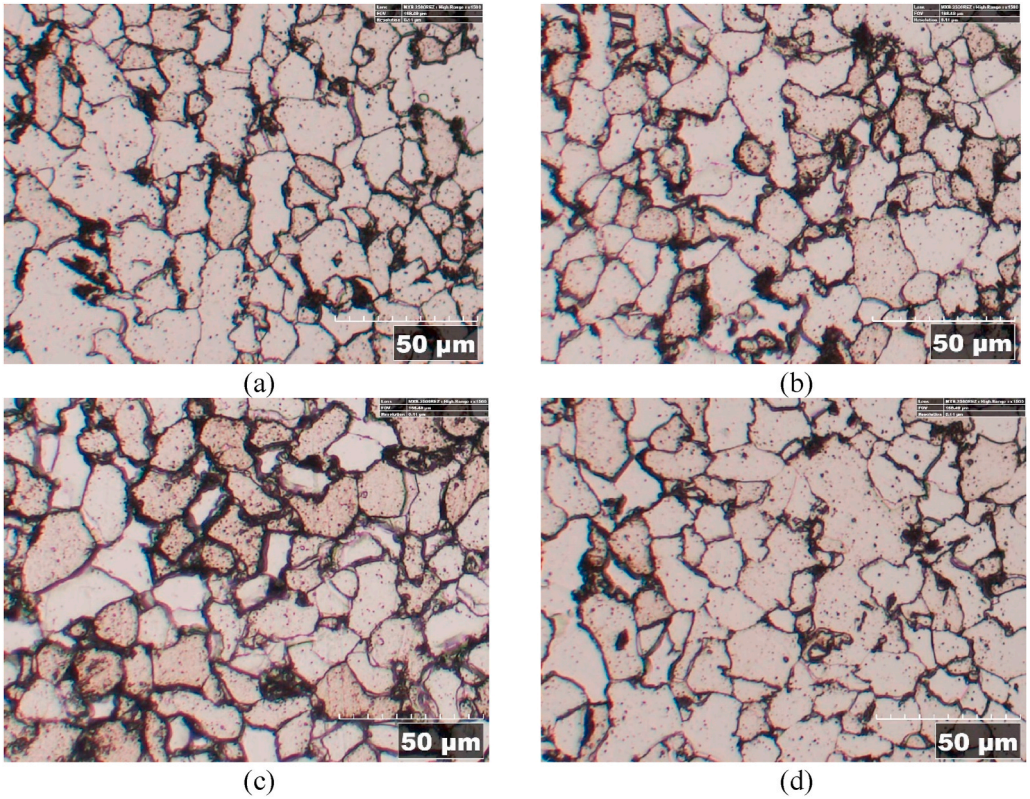


Fig. 11. Typical microstructures of ER70S-6 WAAM specimens in the middle of Paris region: (a) CT-VT, (b) CT-VB, (c) CT-HT, and (d) CT-HB.

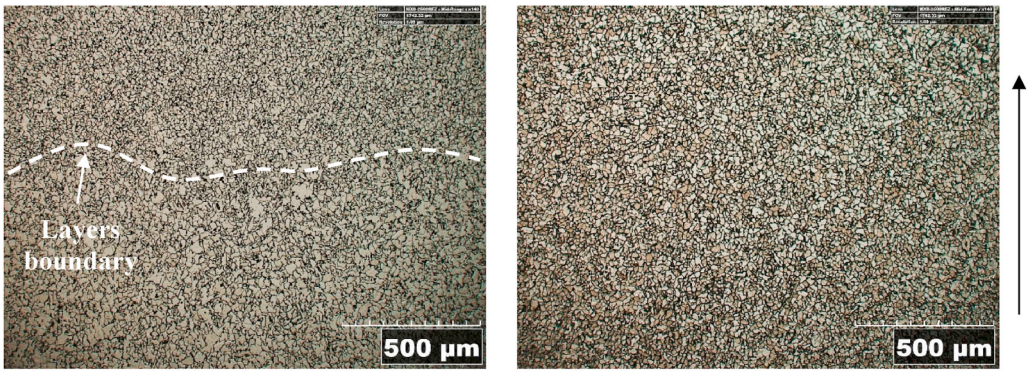


Fig. 12. Comparison of the microstructures for (a) vertical and (b) horizontal specimens (arrow on the right indicates the crack growth direction).

Data availability

Data will be made available on request.

Acknowledgments

This work was supported by grant EP/L016303/1 for Cranfield, Oxford and Strathclyde Universities' Centre for Doctoral Training in Renewable Energy Marine Structures–REMS CDT (http://www.rems-cdt.ac.uk/) from the UK Engineering and Physical Sciences Research Council (EPSRC).

References

Adedipe, O., Brennan, F., Kolios, A., 2015. Corrosion fatigue load frequency sensitivity analysis. Mar. Struct. 42, 115–136.

Adedipe, O., Brennan, F., Kolios, A., 2016. Review of corrosion fatigue in offshore structures: present status and challenges in the offshore wind sector. Renew. Sustain. Energy Rev. 61, 141–154.

Adedipe, O., Brennan, F., Mehmanparast, A., Kolios, A., Tavares, I., 2017. Corrosion fatigue crack growth mechanisms in offshore monopile steel weldments. Fatig. Fract. Eng. Mater. Struct. 40, 1868–1881.

American Society for Testing and Materials, 2011. ASTME-1820-11: standard test method for measurement of fracture toughness. In: Annual Book of ASTM Standards 1–55. https://doi.org/10.1520/E1820-18.

ASTM E647−13, 2014. Standard test method for measurement of fatigue crack growth rates. Am. Soc. Test. Mater. 1–50. https://doi.org/10.1520/E0647-15E01.2.

Bertini, L., 1991. Influence of seawater and residual stresses on fatigue crack growth in CMn steel weld joints. Theor. Appl. Fract. Mech. 16, 135–144.

BS 7910, 2015. BSI Standards Publication Guide to Methods for Assessing the Acceptability of Flaws in Metallic Structures, vol. 490. BSI Standards Publication.

Burnside, O.H., Hudak Jr., S.J., Oelkers, E., Chan, K., Dexter, R.J., 1984. Long-Term Corrosion Fatigue of Welded Marine Steels.

Ermakova, A., Mehmanparast, A., Ganguly, S., 2019. A review of present status and challenges of using additive manufacturing technology for offshore wind applications. Procedia Struct. Integr. 17, 29–36.

Ermakova, A., Mehmanparast, A., Ganguly, S., Razavi, J., Berto, F., 2020. Investigation of mechanical and fracture properties of wire and arc additively manufactured low carbon steel components. Theor. Appl. Fract. Mech. 109, 102685.

Ermakova, A., Mehmanparast, A., Ganguly, S., Razavi, J., Berto, F., 2021. Fatigue crack growth behaviour of wire and arc additively manufactured ER70S-6 low carbon steel components. Int. J. Fract. https://doi.org/10.1007/s10704-021-00545-8.

Fatigue behaviour of high-strength steel-welded joints in offshore and marine systems (FATHOMS) - Publications Office of the EU. https://op.europa.eu/en/publication-detail/-/publication/52679314-1c6d-41d6-9d70-19711b29427f.

Henderson, A., 2003. In: Hydrodynamic Loading of Offshore Wind Turbines.

Hou, C.Y., 2007. Fatigue analysis of welded joints with the aid of real three-dimensional weld toe geometry. Int. J. Fatig. 29, 772–785.

International, A., 2013. D1141-98 standard practice for the preparation of substitute ocean water. ASTM Int. 98, 1–3.

Jacob, A., Mehmanparast, A., 2021. Crack growth direction effects on corrosion-fatigue behaviour of offshore wind turbine steel weldments. Mar. Struct. 75, 102881.

Jacob, A., Mehmanparast, A., D'Urzo, R., Kelleher, J., 2019. Experimental and numerical investigation of residual stress effects on fatigue crack growth behaviour of S355 steel weldments. Int. J. Fatig. 128, 105196.

Liljedahl, C.D.M., Brouard, J., Zanellato, O., Lin, J., Tan, M.L., Ganguly, S., Irving, P.E., Fitzpatrick, M.E., Zhang, X., Edwards, L., 2009. Weld residual stress effects on fatigue crack growth behaviour of aluminium alloy 2024-T351. Int. J. Fatig. 31, 1081–1088.

Lincoln Electric Company, T. LINCOLN ® ER70S–6 WELDING POSITIONS TYPICAL APPLICATIONS. www.lincolnelectric.com.

Martina, F., Mehnen, J., Williams, S.W., Colegrove, P., Wang, F., 2012. Investigation of the benefits of plasma deposition for the additive layer manufacture of Ti–6Al–4V. J. Mater. Process. Technol. 212, 1377–1386.

Mehmanparast, A., Brennan, F., Tavares, I., 2017. Fatigue crack growth rates for offshore wind monopile weldments in air and seawater: SLIC inter-laboratory test results. Mater. Des. 114, 494–504.

Mehmanparast, A., Taylor, J., Brennan, F., Tavares, I., 2018. Experimental investigation of mechanical and fracture properties of offshore wind monopile weldments: SLIC interlaboratory test results. Fatig. Fract. Eng. Mater. Struct. 41, 2485–2501.

Newman, J.C., Yamada, Y., James, M.A., 2011. Back-face strain compliance relation for compact specimens for wide range in crack lengths. Eng. Fract. Mech. 78, 2707–2711.

Practice, S, 2016. Standard Practice for Microetching Metals and Alloys ASTM E-407, vol. 7, pp. 1–22.

Ron, T., Levy, G.K., Dolev, O., Leon, A., Shirizly, A., Aghion, E., 2019. Environmental behavior of low carbon steel produced by a wire arc additive manufacturing process. Metals 9.

Ron, T., Levy, G.K., Dolev, O., Leon, A., Shirizly, A., Aghion, E., 2020. The effect of microstructural imperfections on corrosion fatigue of additively manufactured ER70S-6 alloy produced by wire arc deposition. Metals 10.

Ron, T., Dolev, O., Leon, A., Shirizly, A., Aghion, E., 2021. Effect of phase transformation on stress corrosion behavior of additively manufactured austenitic stainless steel produced by directed energy deposition. Materials 14, 1–12.

Vosikovsky, O., 1980. Effects of stress ratio on fatigue crack growth rates in X70 pipeline steel in air and saltwater. J. Test. Eval. 8.

Williams, S., Martina, W., , F, Addison, A.C., Ding, J., Pardal, G., Colegrove, P., 2015. Wire + arc additive manufacturing. Mater. Sci. Technol. 32, 641–647.

Xu, X., Ganguly, S., Ding, J., Guo, S., Williams, S., Martina, F., 2018. Microstructural evolution and mechanical properties of maraging steel produced by wire + arc additive manufacture process. Mater. Char. 143, 152–162.

Zhang, X., Martina, F., Syed, A.K., Ding, J., 2017. Fatigue Crack Growth in Additive Manufactured Titanium: Residual Stress Control and Life Evaluation Method Development, pp. 7–9. https://doi.org/10.13140/RG.2.2.29032.16643.



https://dspace.org/

Corrosion-fatigue crack growth behaviour of wire arc additively manufactured ER70S-6 steel parts in marine environments

Ermakova, Anna; Ganguly, Supriyo; Razavi, Javad; Berto, Filippo; Mehmanparast, Ali

2022-07-17
Elsevier
https://doi.org/10.1016/j.euromechsol.2022.104739
Ermakova A, Ganguly S, Razavi J, et al., (2022) Corrosion-fatigue crack growth behaviour of wire arc additively manufactured ER70S-6 steel parts in marine environments. European Journal of Mechanics - A/Solids, Volume 96, November-December 2022, Article number 104739

Downloaded from a DSpace repository. https://dspace.org/